Superscaling and neutral current quasielastic neutrino-nucleus scattering

J. E. Amaro,[1] M. B. Barbaro,[2] J. A. Caballero,[3] and T. W. Donnelly[4]

[1]*Departamento de Física Moderna, Universidad de Granada, E-18071 Granada, Spain*

[2]*Dipartimento di Fisica Teorica, Università di Torino and INFN, Sezione di Torino, Via P. Giuria 1, I-10125 Torino, Italy*

[3]*Departamento de Física Atómica, Molecular y Nuclear, Universidad de Sevilla, Apdo. 1065, E-41080 Sevilla, Spain*

[4]*Center for Theoretical Physics, Laboratory for Nuclear Science and Department of Physics, Massachusetts Institute of Technology, Cambridge, Massachusetts 02139, USA*

The superscaling approach is applied to studies of neutral current neutrino reactions in the quasielastic regime. Using input from scaling analyses of electron scattering data, predictions for high-energy neutrino and antineutrino cross sections are given and compared with results obtained using the relativistic Fermi gas model. The influence of strangeness content inside the nucleons in the nucleus is also explored.

I. INTRODUCTION

Inclusive electron scattering at intermediate to high energies from nuclei is known to exhibit the phenomenon of scaling and superscaling [1–7]. At sufficiently high energies, typically at least 500 MeV, one sees that near the quasielastic peak the cross section may be analyzed in terms of a reduced response obtained by division by a suitable N- and Z-weighted single-nucleon electromagnetic cross section and plotted against an appropriate kinematic variable to see the scaling behaviour. First, when the reduced cross section is seen to depend only on this kinematic variable—the scaling variable—and not on the momentum transfer one has scaling of the first kind. Second, if the reduced cross section and scaling variable have been made dimensionless via removal of the momentum scale characteristic of a given nucleus, and the results are seen to be independent of the particular nuclear species, one has scaling of the second kind. When both types of scaling behavior occur one says that the cross sections exhibit superscaling. In the above-cited studies the appropriate reduced cross sections and scaling variables have been discussed in depth.

One finds that in the relevant energy range in the region below the quasielastic (QE) peak, usually called the scaling region, scaling of the second kind is found to be excellent and scaling of the first kind to be quite good. Above the peak scaling of the second kind is good; however, scaling of the first kind is clearly violated. The last occurs for well-understood reasons, namely in that region one has processes other than quasi-free knockout of nucleons playing an important role. Specifically, the most obvious reaction mechanism is that of exciting a nucleon in the nucleus to a delta, which subsequently decays into a nucleon and a pion. Because the elementary cross section for that process is not the elastic eN cross section used in defining the scaling function introduced above, and because the scaling variable used in the usual analysis assumes the kinematics of the elastic process $N \rightarrow N$, rather than of $N \rightarrow \Delta$ which would now be appropriate, it is not surprising that scale breaking occurs. Additionally, meson exchange current effects are known to violate the scaling behavior, although from modeling in this high-energy regime [8–13] their effects appear not to be the dominant ones.

What was appreciated for the first time in recent work [14] is that it is possible to pursue an approach where both the QE process is active (with its reduced response and scaling variable) and the inelastic process in the Δ region is also incorporated (with its corresponding reduced response and scaling variable). We roughly refer to the region of excitation forming a peak that lies above the maximum of the QE response as the "Δ peak," although it should be understood that the modeling actually includes the full inelastic response on a nucleon (resonant plus nonresonant) for kinematics where the $\Delta(1232)$ is dominant.[1] In Ref. [14] it was shown that an excellent representation of the total inclusive electron scattering cross section from the scaling region up to the peak of the Δ region is attained by inverting the procedure. Using the two scaling functions, one for QE scattering and one for the Δ-region, along with the corresponding N- and Z-weighted elastic ($eN \rightarrow eN$) and inelastic ($eN \rightarrow e'\Delta$) electron scattering cross sections one finds excellent agreement with existing high-quality data over a wide range of kinematics and for various nuclear species. Of considerable importance for what was discussed in the rest of Ref. [14] and will be discussed in the present work is the fact that the quality of the analysis requires the phenomenological scaling functions to be quite asymmetric, with relatively long tails extending in the direction of higher energy loss (positive values of the scaling variables). Such is not typically the case with most models, these almost always being more nearly symmetrical about the peak in the scaling function (see, however, Ref. [15] where in at least one case the correct behavior has been obtained in a model). This fact casts considerable doubt on most existing models for high-energy scattering in the QE and Δ regimes if high-quality results (say better than 25%) are desired.

Having met with success in extending the scaling and superscaling analyses from the scaling region, through the QE peak region and into the Δ region, in Ref. [14] the scaling ideas were inverted: given the scaling functions one can just as well multiply by the elementary charge-changing (CC) neutrino

---

[1]For still higher-lying excitations and DIS a different approach must be taken (see, for example, Ref. [6]).

cross sections now to obtain the corresponding CC neutrino and antineutrino cross sections on nuclei for intermediate to high energies in the same region of excitation. Other related work is presented in Refs. [15,16,20]. Given the ability of this scaling approach to reproduce the electron scattering cross sections, in contrast to most direct modeling that fails in detail to do so, we believe that such predictions for the analogous CC neutrino reactions should be very robust. Clearly such results are of relevance for ongoing studies of neutrino reactions and neutrino oscillations in this intermediate-energy regime.

In the present study these scaling and superscaling ideas are carried a step further to include neutral-current (NC) neutrino and antineutrino scattering cross sections, in this case for scattering from ^{12}C. Specifically, the goal is to obtain results using the same analysis as discussed above (and in detail in Ref. [14]) for the reactions $^{12}C(\nu, p)\nu X$, $^{12}C(\bar{\nu}, p)\bar{\nu}X$ involving proton knockout, and $^{12}C(\nu, n)\nu X$, $^{12}C(\bar{\nu}, n)\bar{\nu}X$ involving neutron knockout in the QE regime, the Δ-regime being left for a subsequent study.

A new feature emerges with such a goal in mind, however, and that arises from the fact that when one has an incident lepton, a scattering with exchange of a γ, $W^{\pm}$ or Z^0, and detects the scattered lepton (i.e., a charged lepton), the t-channel exchange of the appropriate boson is controlled. In contrast, when the scattered lepton is a neutrino or antineutrino, and therefore not detected, but instead a knocked-out nucleon is detected, it is the u-channel whose kinematics are controlled (see also Ref. [17] for discussions of this case). Accordingly, in the scaling analysis it is not obvious that the two types of processes are simply related, and therefore to apply the scaling ideas to NC neutrino and antineutrino scattering, in particular for discussions of differential cross sections as in the present work, we first have to address the issue of how the t- and u-channels are related.

The article is organized the following way: in Sec. II we begin with a basic discussion of the t- and u-channel kinematics involved in the semileptonic electroweak processes of interest (Sec. II A) followed by a brief summary in Sec. II B of the cross section formalism and the ideas of scaling when interrelating t- and u-channel processes. To keep the discussions relatively brief in this subsection, the development of the single-nucleon NC neutrino and antineutrino cross sections is placed in an Appendix. For orientation in Sec. II C the relativistic Fermi gas (RFG) model is invoked and its superscaling properties summarized. Then in Sec. III our results are presented and our conclusions are gathered in Sec. IV.

II. GENERAL FORMALISM FOR U-CHANNEL SCATTERING

We begin the general discussion of how t- and u-channel semileptonic reactions are interrelated with a summary of the relevant kinematic variables in the problem.

A. Kinematics

We consider general semileptonic quasifree scattering from nuclei in the Born approximation.
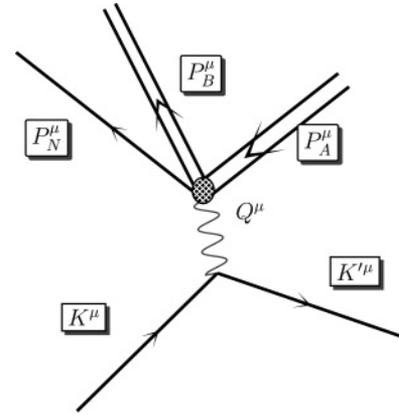

FIG. 1. Kinematics for semileptonic nucleon knockout reactions in the one-boson-exchange approximation.

We start with one basic assumption that is usually presumed to be a good approximation in the kinematic region where quasielastic scattering is dominant, namely that the inclusive cross sections are well represented by the sum of the integrated semi-inclusive proton and neutron emission cross sections. In doing so we are neglecting processes that occur for the same kinematics, but have *no emitted nucleon in the final state* (photon emission, deuteron emission, alpha emission, coherent pion production, etc., but without an emitted nucleon). The process of interest (see Fig. 1) has a lepton of four-momentum $K^{\mu} = (\epsilon, \mathbf{k})$ scattered to another lepton of four-momentum $K'^{\mu} = (\epsilon', \mathbf{k}')$, exchanging a vector boson with four-momentum $Q^{\mu} = K^{\mu} - K'^{\mu}$. The lepton energies are $\epsilon = \sqrt{m^2 + k^2}$ and $\epsilon' = \sqrt{m'^2 + k'^2}$, with m (m') the mass of the initial (final) lepton. For NC neutrino scattering $m = m' = 0$ (assuming zero-mass neutrinos). Note that no assumption such as the plane-wave impulse approximation is being invoked at this stage.

In the laboratory system the initial nucleus is in its ground state with four-momentum $P_A^{\mu} = (M_A^0, 0)$. The final hadronic state corresponds to a nucleon ($N = p$ or n) with four-momentum $P_N^{\mu} = (E_N, \mathbf{p}_N)$ and energy $E_N = \sqrt{m_N^2 + p_N^2}$ plus an unobserved daughter nucleus with four-momentum $P_B^{\mu} = (E_B, \mathbf{p}_B)$. As usual in semileptonic reactions we introduce the missing momentum $\mathbf{p} \equiv -\mathbf{p}_B$ and the excitation energy $\mathcal{E} \equiv E_B - E_B^0$, with $E_B^0 = \sqrt{(M_B^0)^2 + p^2}$, M_B^0 being the ground-state mass of the daughter system (for details see Refs. [2–4]).

For NC neutrino scattering we assume that the neutrino beam momentum is specified and the outgoing nucleon is detected. Hence p_N and the angle θ_{kp_N} (between $\mathbf{k}$ and $\mathbf{p}_N$) are given. Note that the scattered lepton's four-momentum is not specified, as would be the case for t-channel scattering. In analogy with the t-channel case, we can define a u-channel exchanged four-momentum

$$Q'^{\mu} \equiv K^{\mu} - P_N^{\mu} = (\omega', \mathbf{q}'). \tag{1}$$

The above equation yields

$$q' = |\mathbf{q}'| = \sqrt{k^2 + p_N^2 - 2kp_N \cos\theta_{kp_N}}. \tag{2}$$
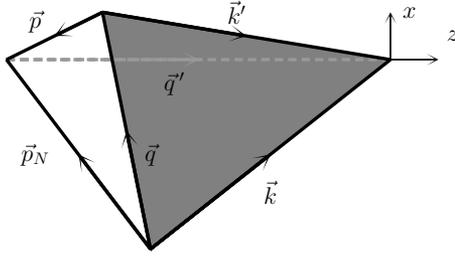
FIG. 2. Vectors relating t-channel and u-channel kinematic variables.

For convenience in looking at the kinematics one can use a coordinate system having the z axis along $\mathbf{q}'$, with $\mathbf{k}$ and $\mathbf{p}_N$ lying in the xz plane. The vectors $\mathbf{k}'$ and $\mathbf{p} = \mathbf{k}' - \mathbf{q}'$ lie in a plane forming an angle ϕ' with the xz plane defined above (see Fig. 2).

The exclusive process illustrated in Fig. 1 is fully determined by six kinematic variables, which can be chosen to be $(k, p_N, \theta_{kp_N}, p, \mathcal{E}, \phi')$. The u-channel inclusive cross section for (k, p_N, θ_{kp_N}) fixed is obtained by integrating over the allowed region in the $(p, \mathcal{E})$ plane and over the azimuthal angle, $0 \leqslant \phi' \leqslant 2\pi$. Again referring to Fig. 2, one sees that at fixed u-channel scattering kinematics (i.e., the triangular region bounded by $\mathbf{k}$, $\mathbf{p}_N$, and $\mathbf{q}'$ fixed) and for a given point in the $(p, \mathcal{E})$ plane, this ϕ' integration corresponds to having the triangle bounded by $\mathbf{p}$, $\mathbf{k}'$, and $\mathbf{q}'$ fixed in size and shape but rotating about the z axis, namely through the full range of the azimuthal angle ϕ'. This clearly implies that the t-channel momentum transfer q varies and that the usual azimuthal angle ϕ (rotations about $\mathbf{q}$) does not cover the full range $(0, 2\pi)$. This has consequences that are discussed in more detail below.

To determine the integration region in the $(p, \mathcal{E})$ plane we use energy conservation, obtaining the following expression:

$$\mathcal{E} = \left(M_A^0 + \omega'\right) - \left[\sqrt{m'^2 + q'^2 + p^2 + 2q'p\cos\theta_{q'p}} + \sqrt{\left(M_B^0\right)^2 + p^2}\right]. \quad (3)$$

Following the usual y-scaling analysis we can now examine the various curves $\mathcal{E} = \mathcal{E}(p)$ that result when various choices are made for $\cos\theta_{q'p}$. Let us call the curves $\mathcal{E}'_\pm(p)$ when $\cos\theta_{q'p} = \pm 1$:

$$\mathcal{E}'_\pm(p) = \left(M_A^0 + \omega'\right) - \left[\sqrt{m'^2 + (q' \pm p)^2} + \sqrt{\left(M_B^0\right)^2 + p^2}\right]. \quad (4)$$

From these we can proceed to find the intersections of the curves with the axis $\mathcal{E} = 0$. This leads to definitions for a scaling variable y' and a maximum missing momentum Y':

$$y' \equiv \frac{1}{W_X^2}\left[\left(M_A^0 + \omega'\right)\sqrt{\Lambda_X^2 - \left(M_B^0\right)^2 W_X^2} - q'\Lambda_X\right] \quad (5)$$

$$Y' \equiv \frac{1}{W_X^2}\left[\left(M_A^0 + \omega'\right)\sqrt{\Lambda_X^2 - \left(M_B^0\right)^2 W_X^2} + q'\Lambda_X\right], \quad (6)$$

where

$$W_X = \sqrt{\left(M_A^0 + \omega'\right)^2 - q'^2} \quad (7)$$

$$\Lambda_X = \tfrac{1}{2}\left[W_X^2 + \left(M_B^0\right)^2 - m'^2\right]. \quad (8)$$

Note that these are new variables and not simply related to the variables y and Y that come from the familiar y-scaling analysis [2–4,7]. The allowed region is then determined: for $y' < 0$ one has $-y' \leqslant p \leqslant Y'$ with $0 \leqslant \mathcal{E} \leqslant \mathcal{E}'_-(p)$, whereas for $y' > 0$ one has for $0 \leqslant p \leqslant y'$ the range $\mathcal{E}'_+(p) \leqslant \mathcal{E} \leqslant \mathcal{E}'_-(p)$ and for $y' \leqslant p \leqslant Y'$ the range $0 \leqslant \mathcal{E} \leqslant \mathcal{E}'_-(p)$. When $y' = 0$ one covers the largest range in missing momentum at the minimal missing energy and accordingly somewhere near this point the inclusive integral is expected to be at a maximum; namely this kinematic point corresponds approximately to the QE peak.

Concerning the azimuthal integration, note that kinematic variables entering the usual t-channel [such as the momentum and energy transfer (q, ω), the lepton scattering angle θ_l between $\mathbf{k}$ and $\mathbf{k}'$, and the solid angle defining the outgoing nucleon momentum (θ_{qp_N}, ϕ_N)] all depend on $\cos\phi'$—see the above discussions of Fig. 2. Thus the integration over ϕ' implies an integration over the azimuthal angle ϕ_N; however, as ϕ' varies, the integration implied over ϕ_N is not being done at constant (q, ω). Furthermore, the range over which the implied ϕ_N integration occurs is not in general the full range. This implies that the symmetry properties of the responses R_K cannot be used in the case of u-channel inclusive scattering to eliminate some of the responses (e.g., the TL and TT terms), as is the case for t-channel inclusive scattering.

B. Cross sections and scaling

Next we turn to a discussion of the basic cross sections and scaling variables involved in the present study. As discussed above we consider only semi-inclusive nucleon knockout reactions in building up the inclusive cross sections. The usual procedure [17] is to start with the plane wave impulse approximation (PWIA) for the $(l, l'N)$ cross section and integrate over all unconstrained kinematic variables. Final-state interactions are then presumed to occur after the primary electroweak interaction with a nucleon in the nucleus and so, for instance, a succession of $(N, 2N)$ steps occurring during the time evolution of the high-energy emitted nucleon as it proceeds through the nuclear medium can cause a redistribution of strength in the missing-energy, missing-momentum plane (see Ref. [25] for recent work along these lines). Such processes tend to move strength from lower missing energies to higher ones and thereby produce an asymmetry in the scaling function, skewing it to larger values of energy loss ω or, equivalently, in the positive scaling variable direction. Other approaches [15] also yield an asymmetric scaling function—in agreement with experiment—when strong final-state interactions are incorporated, again via a shift of strength to higher missing energies.

In contrast, in the present work where our emphasis is placed on interrelating various inclusive semileptonic processes, and not on detailed modeling of the reaction chain, we take as given the full semi-inclusive nucleon knockout cross

section (i.e., given by nature) and proceed to integrate to obtain inclusive cross sections. Clearly this does not imply that we have a full understanding of the former, only that asymptotic states may be used to account for all open channels and that it is not necessary to account for the entire sequence of steps that yields these states.

For t-inclusive scattering, where $Q^\mu \equiv (\omega, \mathbf{q})$ is constant and the final lepton is detected (as in usual inclusive electron scattering or in charge-changing neutrino reactions), the inclusive cross section is calculated by integrating the semi-inclusive cross section $d\sigma/d\Omega_{k'} dk' d\Omega_N dp_N$ over the ejected nucleon (and summing over protons and neutrons), whereas for the u-inclusive scattering we are considering here, where $Q'^\mu \equiv (\omega', \mathbf{q}')$ is constant and the final nucleon is detected, one has to integrate over the final lepton. That is we have

$$\frac{d\sigma}{d\Omega_{k'} dk'} = \int d\Omega_N dp_N \frac{d\sigma}{d\Omega_{k'} dk' d\Omega_N dp_N} \qquad (9)$$

$$\frac{d\sigma}{d\Omega_N dp_N} = \int d\Omega_{k'} dk' \frac{d\sigma}{d\Omega_{k'} dk' d\Omega_N dp_N} \qquad (10)$$

for t- and u-channel reactions, respectively. These integrals can be transformed into integrals in the $(p, \mathcal{E})$ plane using the relations

$$d\Omega_N dp_N = \left(\frac{E_N}{p_N^2}\right) \frac{1}{q} p \, dp \, d\mathcal{E} \, d\phi_N \qquad (11)$$

$$d\Omega_{k'} dk' = \left(\frac{\epsilon'}{k'^2}\right) \frac{1}{q'} p \, dp \, d\mathcal{E} \, d\phi'. \qquad (12)$$

This leads to the following expressions for the inclusive cross sections, in the t-channel

$$\frac{d\sigma}{d\Omega_{k'} dk'} = \frac{2\pi}{q} \int_{\mathcal{D}_t} p \, dp \int d\mathcal{E}$$
$$\times \int_0^{2\pi} \frac{d\phi_N}{2\pi} \left(\frac{E_N}{p_N^2}\right) \frac{d\sigma}{d\Omega_{k'} dk' d\Omega_N dp_N} \qquad (13)$$

and in the u-channel

$$\frac{d\sigma}{d\Omega_N dp_N} = \frac{2\pi}{q'} \int_{\mathcal{D}_u} p \, dp \int d\mathcal{E}$$
$$\times \int_0^{2\pi} \frac{d\phi'}{2\pi} \left(\frac{\epsilon'}{k'^2}\right) \frac{d\sigma}{d\Omega_{k'} dk' d\Omega_N dp_N}, \qquad (14)$$

respectively. The above expressions are simply connected to one other by interchanging the final lepton variables with the final nucleon variables, but for the fact that the integration regions $\mathcal{D}_t$ and $\mathcal{D}_u$ in the $(p, \mathcal{E})$ plane are different in the two cases. The t-channel case is discussed in Ref. [17], whereas the u-channel case is treated in the following section.

To this point we have made only relatively weak approximations by assuming that the cross sections in the quasielastic region are dominated by integrals over the semi-inclusive nucleon knockout cross sections. Following Ref. [17] we write the latter in terms of products of single-nucleon electroweak cross sections multiplied by what may be called the *reduced*

cross section Σ:

$$\frac{d\sigma}{d\Omega_{k'} dk' d\Omega_N dp_N} = \frac{1}{(2\pi)^2} \frac{1}{2\epsilon} \frac{1}{2E} g^4 D_V(Q^2)^2$$
$$\times l_{\mu\nu} w^{\mu\nu} \left(\frac{k'^2}{2\epsilon'}\right) \left(\frac{p_N^2}{2E_N}\right)$$
$$\times \Sigma(q, \omega, \theta_{kk'}, \phi', p, \mathcal{E}), \qquad (15)$$

where E is the energy of the struck nucleon, g is the strength of the fermion-vector boson coupling, and $D_V(Q^2) = (Q^2 - M_V^2)^{-1}$ is the vector boson propagator, whereas $l_{\mu\nu}$ and $w^{\mu\nu}$ are the usual leptonic and (single-nucleon) hadronic tensors, respectively. Clearly other sets of independent variables may be used as arguments of the reduced cross section (see below).

Next we make two stronger approximations. First, we assume that the single-nucleon cross section varies only slowly with $(p, \mathcal{E})$ and may be removed from the integrals over p and $\mathcal{E}$. This has been verified for t-channel reactions as long as the semi-inclusive cross sections are peaked at low missing-energy and missing-momentum (see, for example, Ref. [2]). In particular, for the t-inclusive case the vector boson propagator can be extracted from the integral, and the same applies to the single-nucleon form factors appearing in $w^{\mu\nu}$, as they only depend on Q^2. As a consequence, in t-channel case one can verify that the $(p, \mathcal{E})$ dependence of the single-nucleon cross section is weak at constant (ω, q) and therefore its mean value (namely integrated over ϕ_N and divided by 2π) can be removed from the integrations in Eq. (13). The u-channel case is more complicated and is dealt with below.

If we make this approximation we are left with

$$\frac{d\sigma}{d\Omega_{k'} dk'} \simeq \overline{\sigma}_{sn}^{(t)} F(y, q) \qquad (16)$$

where

$$F(y, q) \equiv \int_{\mathcal{D}_t} p \, dp \int \frac{d\mathcal{E}}{E} \Sigma(q, \omega, \theta_{kk'}, \phi', p, \mathcal{E}) \qquad (17)$$

depends on the scaling variable y and the momentum transfer q [1–4,7]. Note that the reduced cross section Σ occurring above would be the spectral function $S(p, \mathcal{E})$, namely dependent only on $(p, \mathcal{E})$ were the PWIA to be assumed; however, no such assumption is being made here.

Second, we assume *factorization* in the sense that the reduced cross section appearing above depends only weakly on the momentum transfer q, this dependence being contained mostly in the single-nucleon cross section. Note that, for instance, residual dependence in Σ on the scaling variable y is not part of the factorization assumption. Such dependence would not lead to any scaling violation. This means that factorization is not equivalent to assuming dependence only on $(p, \mathcal{E})$ as in the PWIA. Clearly missing here, for instance, are processes involving meson-exchange currents [8–13] that in this sense do not factor, as their dependences on q are clearly not the same as those contained in the single-nucleon cross section that has been divided out to define the reduced cross section. However, our past studies of superscaling show that, for high-energy inclusive scattering at quasielastic kinematics, the scaling behavior is quite well respected, with perhaps 10% or so left to be explained by effects such as those from MEC

that should break the scaling. Indeed, even with relatively strong final-state interactions one finds in some modeling [15] that the scaling is maintained, suggesting that the above assumption is valid, at least in the region of the QE peak.

We note in passing that the violations of scaling of the first kind, namely some residual dependence on the momentum transfer q, even at the level of the above equation can stem from two different sources: (1) the region of integration $\mathcal{D}_t$ depends on q and only for asymptotically high q does it approach a q-independent form, and (2) the reduced cross section Σ may contain some weak dependence on q. Indeed, from the observation that the approach to first-kind scaling is from above, i.e., the measured reduced cross section decreases with q before reaching the scaling domain (see Ref. [2], for example), it appears that (2) must occur, and not just (1), which would imply an approach from below, because the integration region increases with q.

At high energies, where the scaling idea works and scaling of first kind is reasonably good, we find that $F(y, q) \simeq F(y) \equiv F(y, \infty)$ and is not a function of q, in effect validating the factorization assumption and the quality of the approximation where a mean value for the single-nucleon cross section is removed from the integrals. This was used in Ref. [14] to predict the charge-changing (CC) neutrino cross section: we let nature solve for us the integral in Eq. (17) to obtain an empirical function $F(y)$ from electron scattering to be used in CC neutrino studies.

In the u-inclusive case the above factorization is not trivial, because Q^2 varies within the integration region. However, one can again assume that

$$\frac{d\sigma}{d\Omega_N dp_N} \simeq \overline{\sigma}_{sn}^{(u)} F(y', q'), \tag{18}$$

where

$$F(y', q') \equiv \int_{\mathcal{D}_u} p\,dp \int \frac{d\mathcal{E}}{E} \Sigma \simeq F(y'), \tag{19}$$

provided the effective NC single-nucleon cross section

$$\overline{\sigma}_{sn}^{(u)} = \frac{1}{32\pi\epsilon} \frac{1}{q'} \left(\frac{p_N^2}{E_N}\right) g^4 \int_0^{2\pi} \frac{d\phi'}{2\pi}$$
$$\times l_{\mu\nu}(\mathbf{k}, \mathbf{k}')w^{\mu\nu}(\mathbf{p}, \mathbf{p}_N)D_V(Q^2)^2 \tag{20}$$

is almost independent of $(p, \mathcal{E})$ for constant (k, p_N, θ_{kp_N}). This seems indeed to be the case, as shown from numerical studies presented below in Sec. III. Then, as in Ref. [14], the empirically determined scaling function $F(y')$ can be used to predict realistic NC cross sections.

To be able to use the scaling function obtained from analyses of inclusive electron scattering data for predictions of neutrino reaction cross sections one further assumption must be made, namely the domains of integration in the integrals above must be the same or at least very similar. In the case of CC neutrino reactions this is clearly the case except at very low energies for the muon case where the kinematic dependence on the muon mass is important in determining $\mathcal{D}_t$. For NC neutrino reactions the integration domain $\mathcal{D}_u$ differs to some degree from the one that enters in electron scattering, namely $\mathcal{D}_t$. In particular, when determining the

scaling function $F(y', q')$ with input from electron scattering that yields $F(y, q)$, clearly the first step is to use the latter evaluated at $y = y'$ and to work in the scaling regime where q and q' are both large enough to make the regions in the $(p, \mathcal{E})$ plane extend to high p and high $\mathcal{E}$ (see the arguments for electron scattering scaling summarized, for instance, in Ref. [2]). Under these circumstances the regions denoted $\mathcal{D}_t$ and $\mathcal{D}_u$ differ significantly only at large $\mathcal{E}$ (also at large p, but there one believes the semi-inclusive cross sections are negligible). Accordingly, given that the semi-inclusive cross sections are dominated by their behaviors at low $\mathcal{E}$ and low p, one expects the results of the integrations in the two cases, t-channel and u-channel, to be very similar, and thus the scaling functions will be essentially the same. Were this not to be the case, then it would be likely that first-kind scaling for inclusive electron scattering would not occur, in contradiction with observation.

A further difference between the t- and u-scattering cases should be stressed. In both cases the single-nucleon cross section can be expressed in terms of response functions, as shown in the appendix. However, as mentioned above, for t-inclusive processes the special symmetry about the **q** direction can be exploited to remove the TL, TT, and TL′ responses after performing the ϕ_N-integration, which simply yields a factor 2π. In the u-channel, instead, the unrestricted integration over ϕ' yields an effective integration over ϕ_N which is not uniform and does not in general cover all of the interval $(0, 2\pi)$. As a consequence the TL, TT, and TL′ responses do contribute. As shown later, their contribution is suppressed and only the TL contribution is relevant for the kinematics of interest in the present study.

C. RFG and superscaling

In this section we discuss the NC neutrino cross section in the RFG model, which corresponds to the following excitation energy

$$\mathcal{E}_{\mathrm{RFG}}(p) = \sqrt{m_N^2 + k_F^2} - \sqrt{m_N^2 + p^2} \tag{21}$$

and spectral function

$$S_{\mathrm{RFG}}(p, \mathcal{E}) = \frac{3k_F}{4T_F}\theta(k_F - p)\delta[\mathcal{E} - \mathcal{E}_{\mathrm{RFG}}(p)], \tag{22}$$

where k_F is the Fermi momentum and $T_F = \sqrt{k_F^2 + m_N^2} - m_N$ the Fermi kinetic energy.

Because of the delta function in Eq. (22) the integration region in the $(p, \mathcal{E})$ plane simply reduces to a line and the lower limit in the integral over p is given by the intercept of the curve $\mathcal{E}_{\mathrm{RFG}}(p)$ with $\mathcal{E}'_-(p)$ when $y' < 0$. When $y' > 0$ it is given by the intercept of $\mathcal{E}_{\mathrm{RFG}}(p)$ with $\mathcal{E}'_+(p)$ [$\mathcal{E}'_-(p)$] when $\mathcal{E}'_\pm(0) < T_F$ [$\mathcal{E}'_\pm(0) > T_F$]. By solving these equations it is easily shown that the minimum momentum required for a nucleon to participate in the reaction is

$$p_{\min} = \left|y_{\mathrm{RFG}}^{(u)}\right| \tag{23}$$

where

$$y_{\mathrm{RFG}}^{(u)} = s\frac{m_N}{\tau'}[\lambda'\sqrt{\tau'^2\rho'^2 + \tau'} - \kappa'\tau'\rho'] \tag{24}$$
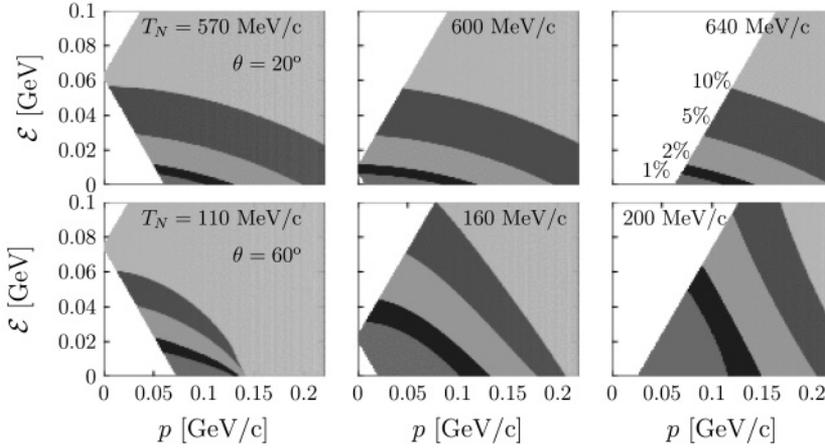
FIG. 3. The various regions correspond to values of the ratio $\mathcal{R} \equiv \overline{\sigma}_{sn}^{(u)}(p, \mathcal{E})/\overline{\sigma}_{sn}^{(u)}(p = |y'|, \mathcal{E} = 0)$ differing from 1 by at most 1 (lowest region), $1-2, 2-5, 5-10$, and more than 10% (highest region). For this figure proton knockout has been assumed; the neutron knockout case is similar and not shown. For brevity, in this figure we let θ stand for the angle θ_{kp_N}.

is the RFG y-scaling variable associated with u-scattering [hence the index (u) to distinguish it from the usual t-channel variable]. Moreover we have introduced the dimensionless kinematic quantities $\kappa' \equiv q'/2m_N$, $\lambda' \equiv \omega'/2m_N$, $\tau' = \kappa'^2 - \lambda'^2$ and defined $\rho' \equiv 1 - \frac{1}{4\tau'}(1 - m'^2/m_N^2)$. The sign s is

$$s \equiv \text{sgn} \left\{ \frac{1}{\tau'} [\lambda' \sqrt{\tau'^2 \rho'^2 + \tau'} - \kappa' \tau' \rho'] \right\}. \quad (25)$$

As in electron scattering, it is convenient to introduce a dimensionless scaling variable

$$\psi_{\text{RFG}}^{(u)} = s \sqrt{\frac{m_N}{T_F}} \left[\sqrt{1 + \left(\frac{y_{\text{RFG}}^{(u)}}{m_N}\right)^2} - 1 \right]^{1/2}, \quad (26)$$

representing the minimum kinetic energy of the nucleons participating in the reaction. By placing the spectral function of Eq. (22) in Eq. (19) one immediately finds the RFG scaling function

$$F_{\text{RFG}}\left(\psi_{\text{RFG}}^{(u)}\right) = \frac{3k_F}{T_F} \int_{E_{\min}}^{E_F} dE \int d\mathcal{E} \, \delta \left(\mathcal{E} - \mathcal{E}_{\text{RFG}}\right)$$
$$= \frac{3}{4} k_F \left(1 - \psi_{\text{RFG}}^{(u)2}\right) \theta \left(1 - \psi_{\text{RFG}}^{(u)2}\right). \quad (27)$$

Providing the single-nucleon cross section is smoothly varying within the $(p, \mathcal{E})$ integration region, the differential RFG cross section can be factorized as shown in Eq. (18) with the scaling function given by Eq. (27). More realistic predictions can be given by using, instead of the RFG scaling function, the empirical scaling function as determined from QE electron scattering, as already done in Ref. [14] for charged current reactions. These are discussed in the next section.

III. RESULTS

Before presenting our predictions for the cross section, we test the validity of the scaling approach in the u-channel. To this end we analyze how the effective NC single-nucleon cross section $\overline{\sigma}_{sn}^{(u)}$ given in Eq. (20) depends on the missing momentum p and excitation energy $\mathcal{E}$ for selected values of the kinematical variables (k, E_N, θ_{kp_N}). To proceed, we assume the proton knockout case and divide $\overline{\sigma}_{sn}^{(u)}$ evaluated in the

whole $(p, \mathcal{E})$-plane by its value corresponding to $p = |y'|$ and $\mathcal{E} = 0$. In what follows we use the cc2 off-shell prescription for the nucleon current and the Höhler parametrization for the single-nucleon form factors [18], ignoring the strangeness content of the nucleon, unless specified otherwise.

The results are given in Fig. 3 in terms of different shadings representing the regions where this ratio differs from unity by at most 1, 1–2, 2–5, 5–10% and more than 10%, respectively, as indicated in the top right panel. The six graphs correspond to two values of the scattering angle θ_{kp_N}: 20^0 (top panels) and 60^0 (bottom panels). In each case, the outgoing proton kinetic energies have been selected to correspond to the regions below, above and close to the peak of the differential cross section. Although not shown here, the results for neutron knockout are very similar to those for proton knockout.

The results in Fig. 3 illustrate the validity of the scaling approach. Only for very large values of the excitation energy does the effective NC single-nucleon cross section depend significantly on $(p, \mathcal{E})$. In fact, restricting ourselves to excitation energies below twice the maximum value of the RFG model, $\mathcal{E} \simeq 50$ MeV, the dispersion presented by the ratio is at most ~ 5–10%.

This outcome is also in accordance with the results presented in Figs. 4 (proton case) and 5 (neutron case). Here we show the neutral current neutrino (upper panels) and antineutrino (lower panels) double differential cross sections for scattering at 1 GeV from ^{12}C as a function of the ejected proton or neutron kinetic energy. The scattering angles have been fixed as in the previous figure.

Beginning with the RFG model, as in past work the Fermi momentum for ^{12}C is taken to be $k_F = 228$ MeV/c and results are given both using the full RFG model (short-dashed curves) and making use of the factorization approach assumed in Eq. (18) with the u-channel NC single-nucleon cross section evaluated at $p = y_{\text{RFG}}$ and $\mathcal{E} = \mathcal{E}_{\text{RFG}}$ (solid lines). One sees that the two sets of results almost coincide in the whole T_N region where the RFG cross section is defined, indicating that the scaling argument works very well.

Hence we may use the phenomenological scaling function extracted from (e, e') data, as was done in our previous CC neutrino reaction analysis (Ref. [14]), to predict NC neutrino-nucleus scattering cross sections. These are also plotted in Figs. 4 and 5 as long-dashed lines: they are seen to be lower by
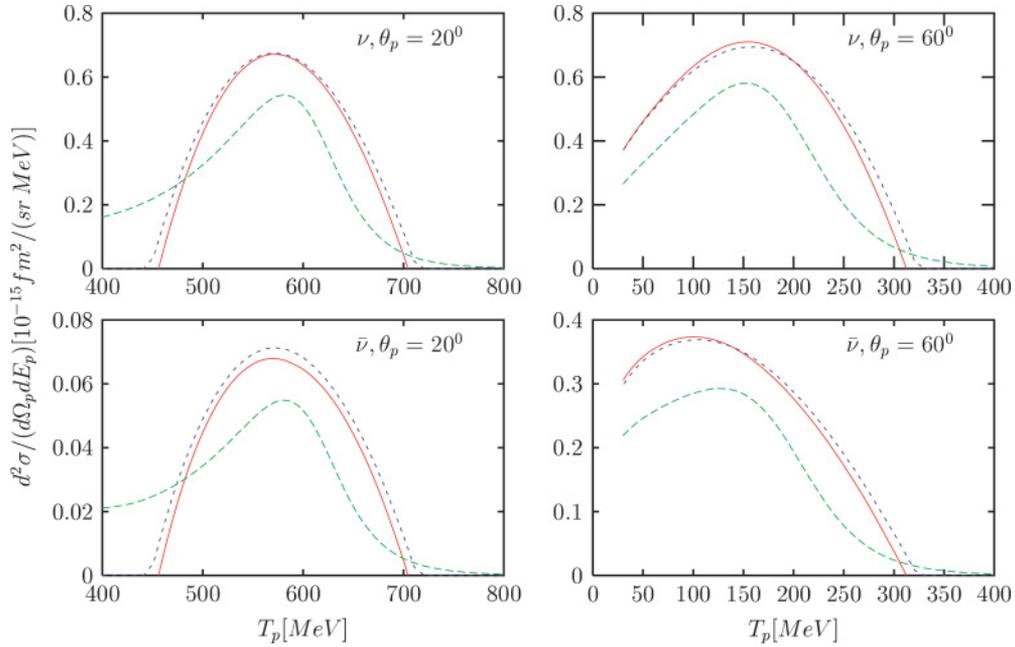
FIG. 4. (Color online) Quasielastic differential cross section for neutral current neutrino and antineutrino scattering at 1 GeV from ^{12}C for proton knockout obtained using the RFG (short-dashed), the factorized approach with the RFG scaling function (solid), and the empirical scaling function (long-dashed). For brevity, in this and in the following figures we let θ_N stand for the angle θ_{kp_N}.

about 25% at the peak than the RFG results, an effect similar to what was found in Ref. [14] for the charge-changing processes. Moreover, the empirical scaling function leads to cross sections extending both below and above the kinematical region where the RFG is defined. In particular, the long tail displayed for low T_N values (corresponding to positive values of the scaling variable ψ') is noteworthy. This tail arises not only from the asymmetric shape of the phenomenological scaling function

but also from the effective NC single-nucleon cross section, which increases significantly for low T_N values.

On comparing Figs. 4 and 5 we see that the shapes of the cross sections for proton and neutron knockout are very similar, although the magnitudes are somewhat different: except for antineutrinos at forward angles, where the cross sections are very small, the neutron knockout results are 30–50% higher than for proton knockout. This occurs because (in absence of
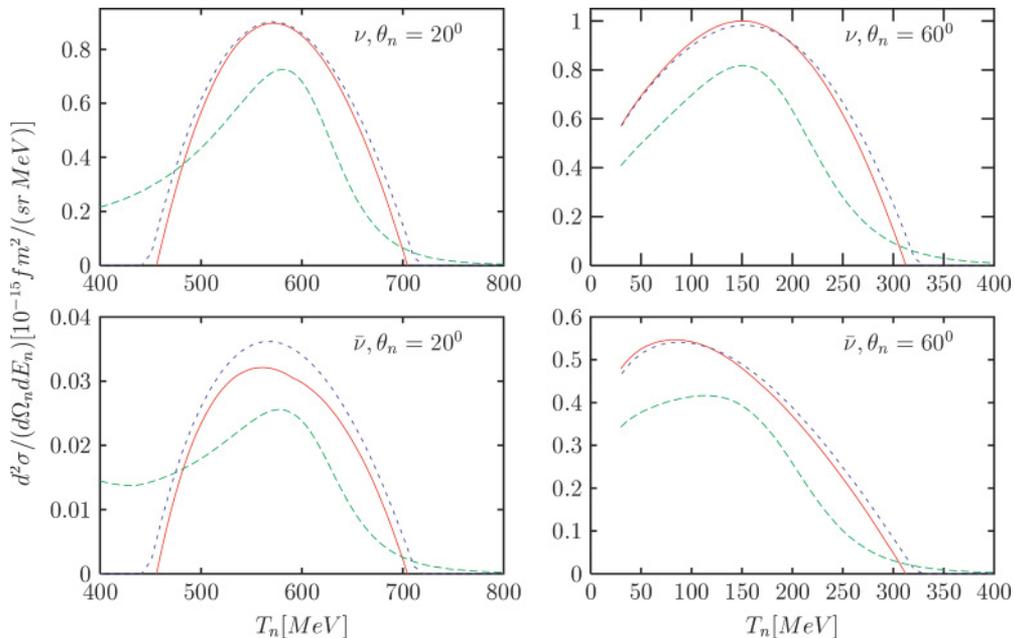

FIG. 5. (Color online) As for the previous figure, but now showing the neutron knockout case.
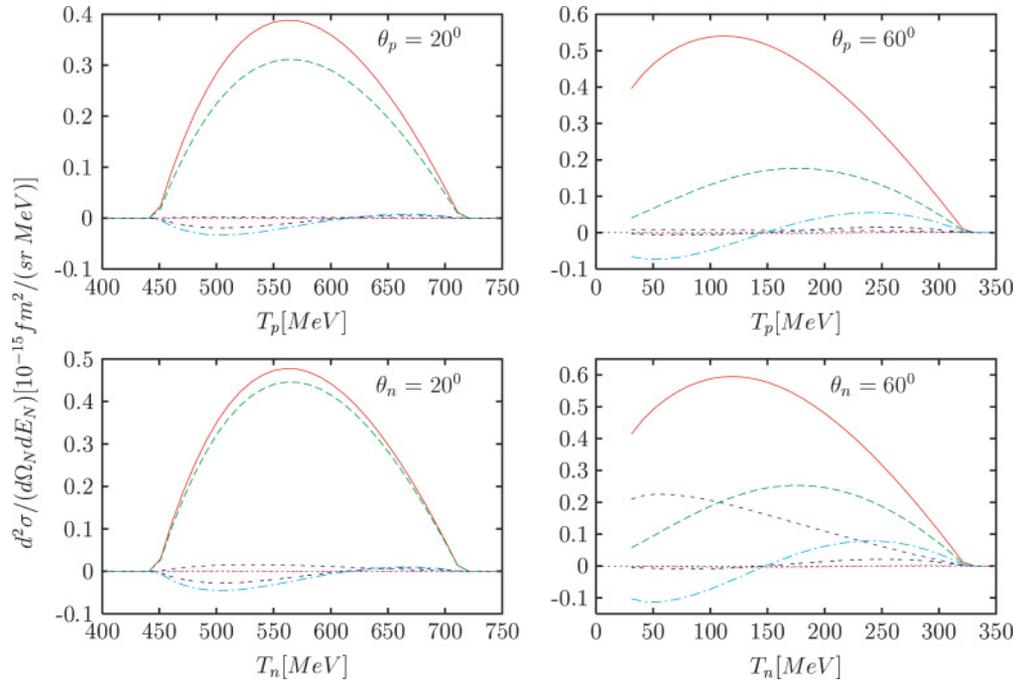
FIG. 6. (Color online) The separate contributions of the response functions of Eqs. (A15)–(A17) to the RFG neutrino cross section: L (short-dashed), T (solid), T' (dashed), TT (dotted), TL (dot-dashed), TL' (double-dashed). The upper panels are for proton knockout and the lower for neutron knockout.

strangeness) both the vector and the axial-vector contributions are larger for neutrons than for protons, and they sum up. In particular, the AA piece is the same for p and n, because $\widetilde{G}_{Ap} = -\widetilde{G}_{An}$ [see Eq. (A33)]. However, from Eqs. (A28), (A29), (A34), and (A35) one has that $\widetilde{G}_{Ep} \simeq -G_{En}$ and $\widetilde{G}_{En} \simeq -G_{Ep}$. Hence, when compared with electromagnetic interactions, the roles of protons and neutrons are reversed in the weak neutral sector, so that $|\widetilde{G}_{En}| \gg |\widetilde{G}_{Ep}|$. Similarly, from Eqs. (A30), (A31), (A36), and (A37) one finds that $|\widetilde{G}_{Mn}| > |\widetilde{G}_{Mp}|$. For antineutrinos things are more delicate, because the VA response has the opposite sign. For instance, for neutron knockout at $\theta_n = 20^0$ the sum VV + AA almost exactly cancels the interference, explaining why the forward angle $\bar{\nu}$ neutron cross section is so small.

In Fig. 6 the contributions of the separate responses to the total RFG cross section are displayed. Clearly the dominant contributions arise from the R_T and $R_{T'}$ responses, and in the case of neutron knockout, from R_L at low values of the kinetic energy. Note, however, that although not dominant (see the discussions in the appendix) the R_{TL} response does provide an important contribution at backward angles. In particular, because it is negative at low kinetic energies and positive at high, it skews the overall cross section to higher values of T_p or T_n. Such an effect is, as discussed above, absent for t-channel scattering where the TL, TL', and TT responses are zero.

Finally, in Figs. 7 (proton knockout case) and 8 (neutron knockout case) we explore the dependence of the cross section on the strangeness content of the nucleon (Refs. [19,21,22]). We compare the results obtained from the phenomenological superscaling function in a situation where no strangeness is assumed (solid line) with the ones obtained including

strangeness in the magnetic (long-dashed) and axial-vector (dotted) form factors, using for $\mu_s = G_M^{(s)}(0)$ a representative value extracted from the recent world studies of PV electron scattering [23] and taking $g_A^s = G_A^{(s)}(0)$ to be -0.2 [24]. The effects from inclusion of electric strangeness are not shown here, because $G_E^{(s)}$ has almost no influence on the full cross sections.

Starting with the proton knockout results in Fig. 7, we see that for the ν case magnetic strangeness tends to decrease the cross section, whereas for $\bar{\nu}$ it has the opposite effect (the forward-angle $\bar{\nu}$ cross sections are rather small and not considered in this discussion). For both ν and $\bar{\nu}$ the axial strange contribution tends to increase the cross section, and so the net effect of incorporating both types of strangeness content is relatively larger in the $\bar{\nu}$ case than in the ν case.

However, for the neutron knockout results shown in Fig. 8 the situation is somewhat different: for ν the roles of magnetic and axial strangeness are reversed from what is seen for proton knockout, an effect that is easily understood by examining the sign changes that occur in going from protons to neutrons (see appendix). Specifically, G_{Mp} and G_{Mn} are opposite in sign, whereas, being isoscalar, $G_M^{(s)}$ is the same for protons and neutrons. Similarly, being isoscalar $G_A^{(s)}$ does not change sign in going from protons to neutrons, whereas, being isovector, $G_A^{(3)}$ does. The $\bar{\nu}$ case is anomalous: in this case the interference VA response tends to cancel the VV + AA contributions. Accordingly, for neutron knockout including magnetic strangeness, which increases both the VV and the VA responses, has little net effect on the cross sections, because the two effects cancel out.
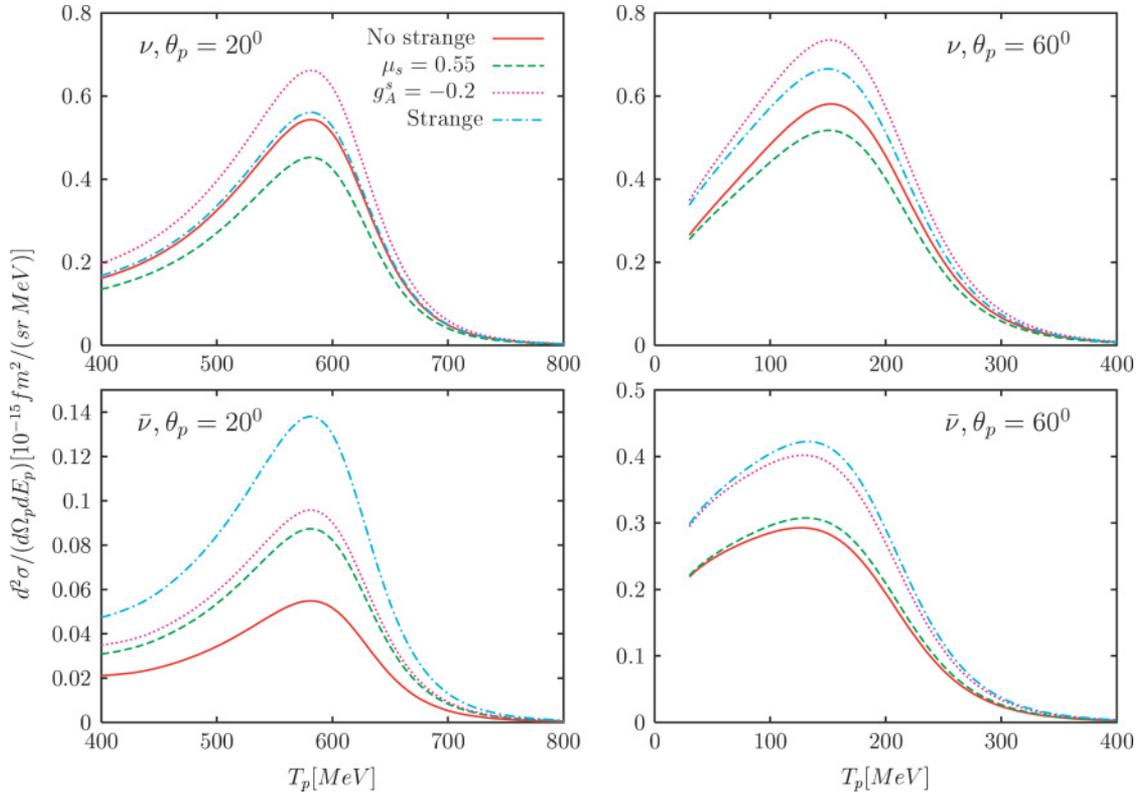
FIG. 7. (Color online) Effects of strangeness and radiative corrections in neutrino and antineutrino cross sections: no strangeness (solid), $\mu_s = 0.55$ (dashed), $g_A^s = -0.2$ (dotted), and all the above effects included (dot-dashed). The case of proton knockout is assumed.
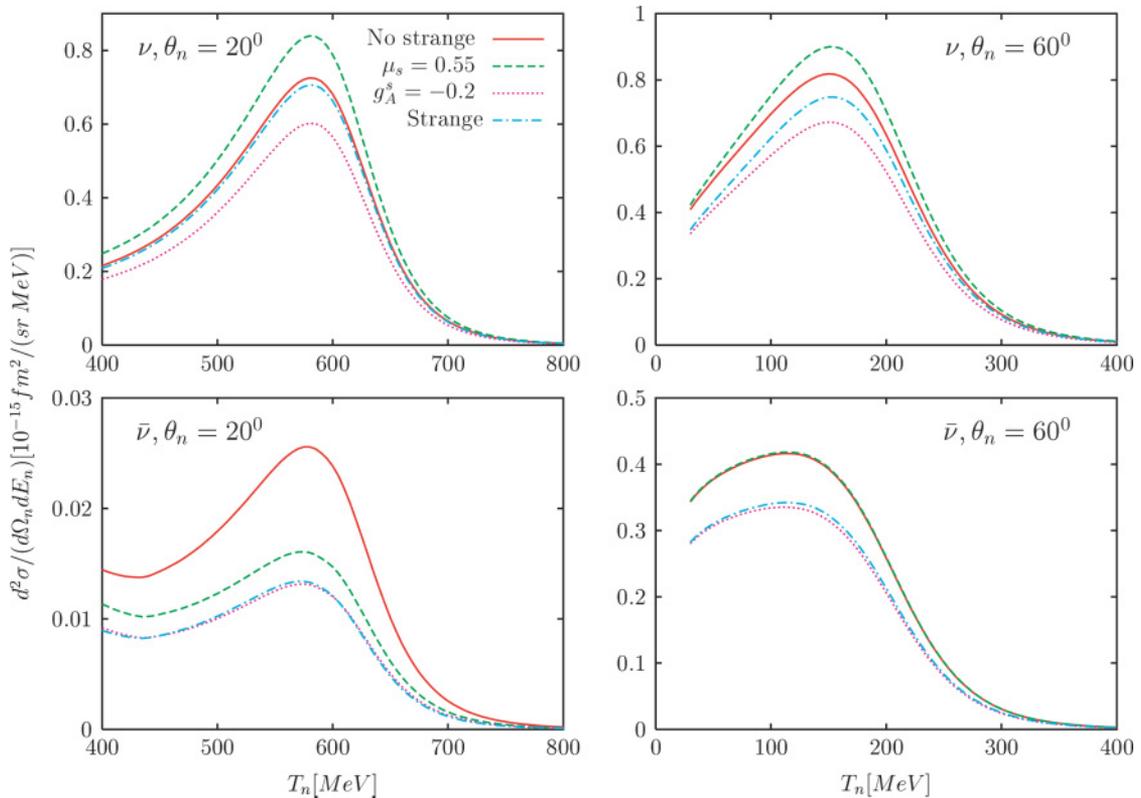

FIG. 8. (Color online) As for the previous figure, but now for neutron knockout.

IV. CONCLUSIONS

In previous work the superscaling formalism was applied to charge-changing neutrino and antineutrino reactions with nuclei. Using QE electron-scattering data, typically at energies above roughly 500 MeV and up to a few GeV, those analyses resulted in a universal scaling function: scaling of both the first and second kinds was demonstrated for the region of excitation lying below the QE peak. This study was supplemented by an analysis of the region lying above the QE peak where the excitation of the nucleon to the $\Delta(1232)$ dominates, and again it was shown that scaling occurs in this domain, albeit with a different scaling function and scaling variable, as expected. Putting these together (two universal scaling functions and two scaling variables, together with the elementary $eN \rightarrow eN$ and $eN \rightarrow e'\Delta$ cross sections) one has a very good representation of inclusive electron scattering at intermediate-to high energies from well below the QE peak up to at least the peak of the Δ-dominated region. Importantly, this high-quality agreement with experiment requires a rather asymmetric scaling function (with a long tail extending to high energy loss) and from other studies undertaken by us and by others it is known that usually the results of modeling yield nearly symmetric scaling functions, clearly at odds with the data. It is then straightforward to insert, instead of the EM cross sections, the elementary CC neutrino and antineutrino cross sections to obtain CC cross sections on nuclei, as discussed in our previous work.

In the present study we have extended that superscaling approach now to include quasielastic scattering via the weak neutral current of neutrinos and antineutrinos from nuclei at intermediate-to-high energies. The same asymmetric QE scaling function and scaling variable employed in the CC study is also used here for the NC predictions, the essential change being simply to insert the NC neutrino and antineutrino νN and $\bar{\nu} N$ cross sections in place of the CC cross sections. Less obvious is the application of the superscaling ideas to the different type of inclusive reaction that must practically be considered. Namely although in the CC reaction studies the relevant reaction involves an incoming lepton (a ν or $\bar{\nu}$) and detection of the corresponding charged lepton at a given scattering angle, just as in electron scattering with incident and scattered electrons (both are t-channel inclusive processes), the NC reaction is different. Here one has an incident ν or $\bar{\nu}$, but now a proton or neutron ejected at some angle, whereas the scattered ν or $\bar{\nu}$ is not detected—this is a so-called u-channel inclusive process. Thus, in the present work we have had to explore the validity of the superscaling ideas when applied to such u-channel scattering, again at intermediate-to-high energies where the scaling approach can be expected to apply. Our results indicate that this is the case and therefore that the scaling analysis used for CC reactions should also work for NC scattering. Additionally, the use of symmetries about the momentum transfer direction in all unpolarized t-channel inclusive processes that leads to only three independent response functions, L, T, and T', is not applicable for u-channel inclusive scattering. There one has in addition the remaining responses TL, TL', and TT, which cannot be eliminated using symmetry arguments. The results

obtained in the present work show that of these only the TL response appears to play a significant role, at least for the kinematics chosen here.

In the present work scattering of neutrinos and antineutrinos at 1 GeV from ^{12}C has been taken as representative and also because it is relevant for ongoing neutrino oscillation experiments. Cross sections at other kinematics and for other nuclei may be obtained by contacting the collaboration. Several conclusions emerge from examining the results obtained.

First, the NC neutrino and antineutrino cross sections are seen to be in roughly a 2:1 ratio (ν:$\bar{\nu}$) at backward νN scattering angles, whereas at forward-scattering angles the antineutrino cross sections are suppressed by an order of magnitude or more. This holds true for both proton and neutron knockout; moreover, the neutron knockout cross sections are somewhat larger than the proton knockout cross sections because of the NC single-nucleon form factors that enter in the two cases (see text for details). These results are also rather different from the corresponding CC reactions where it was observed that, for the kinematics chosen, the antineutrino cross sections are typically much smaller than for neutrinos.

Second, the interplay of the various responses (L, T, TL, TT, T', and TL') is not trivial: in the various channels, ν and $\bar{\nu}$, proton and neutron knockout, they play different roles. For example, the TL response is negative at low nucleon knockout energies and positive at high energies, producing a shift of the total cross sections to higher energies than would occur with only the "usual" responses L, T, and T'.

Finally, the effects of strangeness are relatively large and different for the various channels, implying, as in past studies, that high-quality measurements with ν and $\bar{\nu}$ together with proton and neutron knockout hold the potential to yield more information on the strangeness content of the nucleon.

In summary, the current study employs the same superscaling approach used previously for CC neutrino reactions now applying it to NC neutrino scattering in the QE region. Building in the correct scaling function, in contrast to direct modeling, which usually fails to some degree when applied to electron scattering and therefore must surely fail to the same degree when applied to other semileptonic processes, is an essential ingredient in this approach. In ongoing work our intent is to incorporate u-channel inclusive cross sections for excitations in the Δ region and beyond as in our previous work; however, such investigations are more involved than the QE study presented here, because the final state involves both a nucleon and a pion, and thus are postponed to the future.

APPENDIX: SINGLE-NUCLEON CROSS SECTION

In this appendix we provide the elementary cross section for the reaction

$$\nu(\bar{\nu})N \rightarrow \nu(\bar{\nu})N. \tag{A1}$$

The single-nucleon cross section $\sigma \sim l_{\mu\nu}w^{\mu\nu}$ is given in term of the leptonic tensor (assuming $m = m' = 0$)

$$l_{\mu\nu} = K_\mu K'_\nu + K'_\mu K_\nu - (KK')g_{\mu\nu} + i\chi\epsilon_{\mu\nu\alpha\beta}K^\alpha K'^\beta \tag{A2}$$

with $\chi = +1$ for neutrinos and -1 for antineutrinos, and of the hadronic tensor

$$w^{\mu\nu} = w_S^{\mu\nu} + w_A^{\mu\nu}. \tag{A3}$$

This can be decomposed into a symmetric

$$w_S^{\mu\nu} = w_{VV}^{\mu\nu} + w_{AA}^{\mu\nu} \tag{A4}$$

$$w_{VV}^{\mu\nu} = -w_{1V}(\tau)\left(g^{\mu\nu} + \frac{\kappa^\mu \kappa^\nu}{\tau}\right) + w_{2V}(\tau)X^\mu X^\nu \tag{A5}$$

$$w_{AA}^{\mu\nu} = -w_{1A}(\tau)\left(g^{\mu\nu} + \frac{\kappa^\mu \kappa^\nu}{\tau}\right) + w_{2A}(\tau)X^\mu X^\nu$$
$$- u_{1A}(\tau)\frac{\kappa^\mu \kappa^\nu}{\tau} + u_{2A}(\tau)(\kappa^\mu \eta^\nu + \eta^\mu \kappa^\nu) \tag{A6}$$

and an antisymmetric

$$w_A^{\mu\nu} = w_{VA}^{\mu\nu} = 2iw_3(\tau)\epsilon^{\mu\nu\alpha\beta}\eta_\alpha \kappa_\beta + w_4(\tau)(\kappa^\mu \eta^\nu - \eta^\mu \kappa^\nu) \tag{A7}$$

tensor, where

$$X^\mu \equiv \eta^\mu + \frac{\eta \cdot \kappa}{\tau}\kappa^\mu \overset{on-shell}{=} \eta^\mu + \kappa^\mu \tag{A8}$$

having introduced the dimensionless variables $\kappa^\mu \equiv (\lambda, \boldsymbol{\kappa}) = Q^\mu/2m_N$, $\eta^\mu = P^\mu/m_N$, $\tau = \kappa^2 - \lambda^2$. Note that u_{1A} (the pseudoscalar term), u_{2A}, and w_4 do not contribute to $l_{\mu\nu}w^{\mu\nu}$, because

$$l_{\mu\nu}\kappa^\mu = (K_\mu K'_\nu + K'_\mu K_\nu - g_{\mu\nu}KK')(K^\mu - K'^\mu) = 0 \tag{A9}$$

and

$$l_{\mu\nu}\kappa^\nu = (K_\mu K'_\nu + K'_\mu K_\nu - g_{\mu\nu}KK')(K^\nu - K'^\nu) = 0 \tag{A10}$$

if the leptons are massless. By contracting the above tensors we get

$$l_{\mu\nu}w^{\mu\nu} = x_0 \{v_L R_L + v_T R_T + v_{TT} R_{TT} + v_{TL} R_{TL} + \chi(2v_{T'} R_{T'} + 2v_{TL'} R_{TL'})\} \tag{A11}$$

where $x_0 \equiv 2\epsilon\epsilon' \cos^2\theta_l/2$, θ_l is the lepton scattering angle, $\rho \equiv \tau/\kappa^2$ and

$$v_L = \rho^2 \quad v_T = \frac{1}{2}\rho + \tan^2\frac{\theta_l}{2}, \quad v_{TT} = -\frac{1}{2}\rho \tag{A12}$$

$$v_{TL} = -\frac{1}{\sqrt{2}}\rho\sqrt{\rho + \tan^2\frac{\theta_l}{2}} \tag{A13}$$

$$v_{T'} = \tan\frac{\theta_l}{2}\sqrt{\rho + \tan^2\frac{\theta_l}{2}}, \quad v_{TL'} = -\frac{1}{\sqrt{2}}\rho\tan\frac{\theta_l}{2}. \tag{A14}$$

The response functions are

$$R_L = w^{00}, \quad R_T = w^{11} + w^{22}, \quad R_{TT} = w^{22} - w^{11} \tag{A15}$$

$$R_{TL} = \sqrt{2}(w^{01} + w^{10}) \tag{A16}$$

$$R_{T'} = iw^{21}, \quad R_{TL'} = i\sqrt{2}w^{20}. \tag{A17}$$

In terms of the structure functions w_1, w_2, w_3 the above response functions read (for on-shell nucleons, $\eta \cdot \kappa = \tau$):

$$R_L = -w_1(\tau)\frac{\kappa^2}{\tau} + w_2(\tau)(\varepsilon + \lambda)^2 \tag{A18}$$

$$R_T = 2w_1(\tau) + w_2(\tau)\eta^2 \sin^2\theta \tag{A19}$$

$$R_{TT} = -w_2(\tau)\eta^2 \sin^2\theta \cos(2\phi) \tag{A20}$$

$$R_{TL} = 2\sqrt{2}w_2(\tau)(\varepsilon + \lambda)\eta \sin\theta \cos\phi \tag{A21}$$

$$R_{T'} = 2w_3(\tau)\frac{\tau}{\kappa}(\varepsilon + \lambda) \tag{A22}$$

$$R_{TL'} = 2\sqrt{2}w_3(\tau)\kappa\eta \sin\theta \cos\phi \tag{A23}$$

where the angles θ and ϕ define the bound-nucleon direction with respect to the reference system used in the t-channel (**q** along the z axis), its energy being $\varepsilon \equiv E/m_N$. Note that in this system $\phi = \phi_N$ (the outgoing nucleon's azimuthal angle).

In the usual t-channel inclusive scattering the TT, TL, and TL' responses vanish, because they are integrated over the azimuthal angle ϕ throughout the full range $(0, 2\pi)$; however, this does not occur in u-channel inclusive processes, where the integration over the outgoing lepton implies an integration over the full range of ϕ', but not of ϕ. From Eqs. (A17)–(A22) we see that two of the responses are proportional to the small bound-nucleon momentum parameter $\eta \cong 1/4$; namely R_{TL} and $R_{TL'}$ are both $O(\eta)$ and therefore vanish in the limit $\eta \rightarrow 0$. Accordingly, the TL and TL' responses are expected to be smaller than the L, T, and T' responses that survive in the limit $\eta \rightarrow 0$. However, because R_{TT} is $O(\eta^2)$, one expects that the TT contributions should be the smallest, as is verified by examining the results in Sec. III.

In terms of single-nucleon form factors the structure functions are ($a = p, n$):

$$w_{1a}(\tau) = \tau\widetilde{G}_{Ma}^2(\tau) + (1 + \tau)\widetilde{G}_{Aa}^2(\tau) \tag{A24}$$

$$w_{2a}(\tau) = \frac{\widetilde{G}_{Ea}^2(\tau) + \tau\widetilde{G}_{Ma}^2(\tau)}{1 + \tau} + \widetilde{G}_{Aa}^2(\tau) \tag{A25}$$

$$w_{3a}(\tau) = \widetilde{G}_{Ma}(\tau)\widetilde{G}_{Aa}(\tau) \tag{A26}$$

where [24]

$$\widetilde{G}_{Ep}(\tau) = (2 - 4\sin^2\theta_W)G_E^{T=1}(\tau)$$
$$- 4\sin^2\theta_W G_E^{T=0}(\tau) - G_E^{(s)}(\tau) \tag{A27}$$

$$\widetilde{G}_{En}(\tau) = -(2 - 4\sin^2\theta_W)G_E^{T=1}(\tau)$$
$$- 4\sin^2\theta_W G_E^{T=0}(\tau) - G_E^{(s)}(\tau) \tag{A28}$$

$$\widetilde{G}_{Mp}(\tau) = (2 - 4\sin^2\theta_W)G_M^{T=1}(\tau)$$
$$- 4\sin^2\theta_W G_M^{T=0}(\tau) - G_M^{(s)}(\tau) \tag{A29}$$

$$\widetilde{G}_{Mn}(\tau) = -(2 - 4\sin^2\theta_W)G_M^{T=1}(\tau)$$
$$- 4\sin^2\theta_W G_M^{T=0}(\tau) - G_M^{(s)}(\tau) \tag{A30}$$

$$\widetilde{G}_{Ap}(\tau) = -2G_A^{(3)}(\tau) + G_A^{(s)}(\tau) \tag{A31}$$

$$\widetilde{G}_{An}(\tau) = 2G_A^{(3)}(\tau) + G_A^{(s)}(\tau). \tag{A32}$$

In the above

$$G_E^{T=0}(\tau) = \tfrac{1}{2}[G_{Ep}(\tau) + G_{En}(\tau)] \tag{A33}$$

$$G_E^{T=1}(\tau) = \tfrac{1}{2}[G_{Ep}(\tau) - G_{En}(\tau)] \tag{A34}$$

$$G_M^{T=0}(\tau) = \tfrac{1}{2}[G_{Mp}(\tau) + G_{Mn}(\tau)] \tag{A35}$$

$$G_M^{T=1}(\tau) = \tfrac{1}{2}[G_{Mp}(\tau) - G_{Mn}(\tau)] \tag{A36}$$

are the electromagnetic isoscalar and isovector Sachs form factors, whereas the isovector axial-vector form factor is given by

$$G_A^{(3)}(\tau) = \tfrac{1}{2}(D + F)G_A^D(\tau) \tag{A37}$$

with $D = 1.262/1.64$, $F = 0.64D$, and $G_A^D(\tau) = (1 + 3.32\tau)^{-2}$.

The strangeness form factors are parametrized as follows:

$$G_E^{(s)}(\tau) = \rho_s \tau G_V^D(\tau) \tag{A38}$$

$$G_M^{(s)}(\tau) = \mu_s G_V^D(\tau) \tag{A39}$$

$$G_S^{(s)}(\tau) = g_A^s G_A^D(\tau), \tag{A40}$$

with $G_V^D(\tau) = (1 + 4.97\tau)^{-2}$.

[1] W. M. Alberico, A. Molinari, T. W. Donnelly, E. L. Kronenberg, and J. W. Van Orden, Phys. Rev. C **38**, 1801 (1988).

[2] D. B. Day, J. S. McCarthy, T. W. Donnelly, and I. Sick, Annu. Rev. Nucl. Part. Sci. **40**, 357 (1990).

[3] T. W. Donnelly and I. Sick, Phys. Rev. Lett. **82**, 3212 (1999).

[4] T. W. Donnelly and I. Sick, Phys. Rev. C **60**, 065502 (1999).

[5] C. Maieron, T. W. Donnelly, and I. Sick, Phys. Rev. C **65**, 025502 (2002).

[6] M. B. Barbaro, J. A. Caballero, T. W. Donnelly, and C. Maieron, Phys. Rev. C **69**, 035502 (2004).

[7] M. B. Barbaro, R. Cenni, A. De Pace, T. W. Donnelly, and A. Molinari, Nucl. Phys. **A643**, 137 (1998).

[8] J. E. Amaro, M. B. Barbaro, J. A. Caballero, T. W. Donnelly, and A. Molinari, Phys. Rep. **368**, 317 (2002).

[9] J. E. Amaro, M. B. Barbaro, J. A. Caballero, T. W. Donnelly, and A. Molinari, Nucl. Phys. **A697**, 388 (2002).

[10] J. E. Amaro, M. B. Barbaro, J. A. Caballero, T. W. Donnelly, and A. Molinari, Nucl. Phys. **A723**, 181 (2003).

[11] J. E. Amaro, M. B. Barbaro, J. A. Caballero, T. W. Donnelly, and A. Molinari, Nucl. Phys. **A643**, 349 (1998).

[12] A. De Pace, M. Nardi, W. M. Alberico, T. W. Donnelly, and A. Molinari, Nucl. Phys. **A726**, 303 (2003).

[13] A. De Pace, M. Nardi, W. M. Alberico, T. W. Donnelly, and A. Molinari, Nucl. Phys. **A741**, 249 (2004).

[14] J. E. Amaro, M. B. Barbaro, J. A. Caballero, T. W. Donnelly, A. Molinari, and I. Sick, Phys. Rev. C **71**, 015501 (2005).

[15] J. A. Caballero, J. E. Amaro, M. B. Barbaro, T. W. Donnelly, C. Maieron, and J. M. Udias, Phys. Rev. Lett. **25**, 252502 (2005).

[16] J. E. Amaro, M. B. Barbaro, J. A. Caballero, T. W. Donnelly, and C. Maieron, Phys. Rev. C **71**, 065501 (2005).

[17] M. B. Barbaro, A. De Pace, T. W. Donnelly, A. Molinari, and M. J. Musolf, Phys. Rev. C **54**, 1954 (1996).

[18] G. Höhler et al., Nucl. Phys. **B114**, 505 (1976).

[19] W. M. Alberico et al., Nucl. Phys. **A651**, 277 (1999); W. M. Alberico et al., Phys. Lett. **B438**, 9 (1998); W. M. Alberico et al., Nucl. Phys. **A623**, 471 (1997).

[20] C. Maieron, M. C. Martinez, J. A. Caballero, and J. M. Udias, Phys. Rev. C **68**, 048501 (2003).

[21] W. M. Alberico, S. M. Bilenky, and C. Maieron, Phys. Rep. **358**, 227 (2002).

[22] A. Meucci, C. Giusti, and F. D. Pacati, Nucl. Phys. **A744**, 307 (2004).

[23] K. A. Aniol et al. (HAPPEX Collaboration), arXiv: nucl-ex/0506011; Phys. Rev. Lett. **96**, 022003 (2006) [arXiv: nucl-ex/0506010]; D. S. Armstrong et al. (G0 Collaboration), Phys. Rev. Lett. **95**, 092001 (2005).

[24] M. J. Musolf, T. W. Donnelly, J. Dubach, S. J. Pollock, S. Kowalski, and E. J. Beise, Phys. Rep. **239**, 1 (1994); see also T. W. Donnelly and R. D. Peccei, Phys. Rep. **50**, 1 (1979).

[25] J. Nieves, M. Valverde, and M. J. Vicente Vacas, Phys. Rev. C **73**, 025504 (2006) [arXiv: hep-ph/0511204].